



Cite this: *Chem. Commun.*, 2015, 51, 4689

Received 8th January 2015,
Accepted 11th February 2015

DOI: 10.1039/c5cc00038f

www.rsc.org/chemcomm

$[(\text{Li}_{0.8}\text{Fe}_{0.2})\text{OH}]\text{FeS}$ and the ferromagnetic superconductors $[(\text{Li}_{0.8}\text{Fe}_{0.2})\text{OH}]\text{Fe}(\text{S}_{1-x}\text{Se}_x)$ ($0 < x \leq 1$)[†]

U. Pachmayr and D. Johrendt*

Superconductivity up to 43 K and magnetic ordering coexist in the iron chalcogenides $[(\text{Li}_{0.8}\text{Fe}_{0.2})\text{OH}]\text{Fe}(\text{S}_{1-x}\text{Se}_x)$ ($0 < x \leq 1$). Substitution of sulphur for selenium gradually suppresses superconductivity while the ferromagnetic signature persists up to non-superconducting $[(\text{Li}_{0.8}\text{Fe}_{0.2})\text{OH}]\text{FeS}$.

A conclusive understanding of unconventional superconductivity in correlated electron systems is among the most challenging topics in contemporary solid state chemistry and physics.¹ In copper-oxide² and iron-based³ materials, superconductivity emerges close to the disappearance of an antiferromagnetically ordered state^{4,5} leading to the assumption that magnetism plays a crucial role in the formation of the Cooper pairs.⁶ In contrast, superconductivity is generally considered incompatible with ferromagnetism. The latter generates magnetic flux, while superconductivity expels magnetic flux from the interior of a solid. Nevertheless, a few examples where both orders coexist are known (see ref. 1–14 in ref. 7). However, a detailed examination of these coexistence phenomena is mostly aggravated by extremely low transition temperatures, as well as by the chemical inertness of the rare-earth 4f shell.

Recently we reported the ferromagnetic iron selenide superconductor $[(\text{Li}_{1-x}\text{Fe}_x)\text{OH}](\text{Fe}_{1-y}\text{Li}_y)\text{Se}$.⁷ The crystal structure exhibits alternately stacked lithium–iron–hydroxide layers and iron selenide layers, and was contemporaneously observed by Lu *et al.*⁸ and Sun *et al.*⁹ Electron doping of the FeSe layer is most probably the main reason for the enormous increase of T_c from 8 K in $\beta\text{-FeSe}$ ¹⁰ to 43 K in $[(\text{Li}_{1-x}\text{Fe}_x)\text{OH}](\text{Fe}_{1-y}\text{Li}_y)\text{Se}$. Similar effects were found in other intercalated iron selenides like $\text{Li}_x(\text{NH}_2)_y(\text{NH}_3)_{1-y}\text{Fe}_2\text{Se}_2$ (ref. 11) or $\text{Li}_x(\text{C}_5\text{H}_5\text{N})_y\text{Fe}_{2-2x}\text{Se}_2$.¹² However, the coexistence of unconventional superconductivity

and ferromagnetism in $[(\text{Li}_{1-x}\text{Fe}_x)\text{OH}](\text{Fe}_{1-y}\text{Li}_y)\text{Se}$ is exceptional. Even though the internal dipole field of the ferromagnet acts on the superconductor, superconductivity is not suppressed and possibly a spontaneous vortex phase is formed. Gathering control over one of these order parameters would give the opportunity to examine the competition, coexistence and coupling of ferromagnetism and superconductivity in more detail.

In this communication we present the chalcogenides $[(\text{Li}_{0.8}\text{Fe}_{0.2})\text{OH}]\text{Fe}(\text{S}_{1-x}\text{Se}_x)$ ($0 \leq x < 1$). We show that the gradual substitution of selenium by sulphur reduces the critical temperature until superconductivity is absent in the pure sulphide, while the ferromagnetic signature persists. Recently Lu *et al.* have interpreted similar data of $[(\text{Li}_{0.8}\text{Fe}_{0.2})\text{OH}]\text{Fe}(\text{S}_{1-x}\text{Se}_x)$ as canted antiferromagnetism.¹³

Polycrystalline samples of $[(\text{Li}_{0.8}\text{Fe}_{0.2})\text{OH}]\text{Fe}(\text{S}_{1-x}\text{Se}_x)$ were synthesized under hydrothermal conditions.^{7†} Iron metal (0.0851 g), $\text{LiOH}\cdot\text{H}_2\text{O}$ (3 g) and appropriate amounts of thiourea respectively selenourea were mixed with distilled water (10 mL). The starting mixtures were tightly sealed in a Teflon-lined steel autoclave (50 mL) and heated at 155 °C for 7 days. After washing with distilled water and ethanol, the polycrystalline products were dried at room temperature under dynamic vacuum and stored at –25 °C under argon atmosphere. Structural characterization by X-ray powder diffraction (PXRD) revealed single phase samples of $[(\text{Li}_{0.8}\text{Fe}_{0.2})\text{OH}]\text{Fe}(\text{S}_{1-x}\text{Se}_x)$ which is isostructural to the selenide.^{7–9} Fig. 1 shows the X-ray powder pattern with Rietveld-fit as well as the crystal structure of $[(\text{Li}_{0.8}\text{Fe}_{0.2})\text{OH}]\text{FeS}$.

The tetragonal structure consists of *anti*-PbO type layers of lithium–iron–hydroxide alternating with FeS layers. X-ray single crystal analysis confirms the structure. Crystallographic data as well as further X-ray powder patterns for $x > 0$ are compiled in the ESI.[†] The compositions of all compounds were confirmed combining energy dispersive X-ray spectroscopy (EDX) measurements, inductively coupled plasma (ICP) analysis and elementary analysis. Remarkably, the composition of the $(\text{Li}_{1-x}\text{Fe}_x)\text{OH}$ layer is the same as in $[(\text{Li}_{1-x}\text{Fe}_x)\text{OH}](\text{Fe}_{1-y}\text{Li}_y)\text{Se}$ ^{7–9} which suggests the same charge transfer of 0.2 electrons in the sulphide. An open

Department Chemie, Ludwig-Maximilians-Universität München, Butenandtstrasse 5-13 (Haus D), 81377 München, Germany. E-mail: johrendt@lmu.de

[†] Electronic supplementary information (ESI) available: Table of crystallographic data, X-ray powder patterns of $[(\text{Li}_{0.8}\text{Fe}_{0.2})\text{OH}]\text{Fe}(\text{S}_{1-x}\text{Se}_x)$ ($0 \leq x \leq 1$), plots showing the evolution of Fe–Ch distances and Ch–Fe–Ch bond angles with x , and Curie–Weiss fit for $[(\text{Li}_{0.8}\text{Fe}_{0.2})\text{OH}]\text{FeS}$. CCDC 1042357. For ESI and crystallographic data in CIF or other electronic format see DOI: 10.1039/c5cc00038f



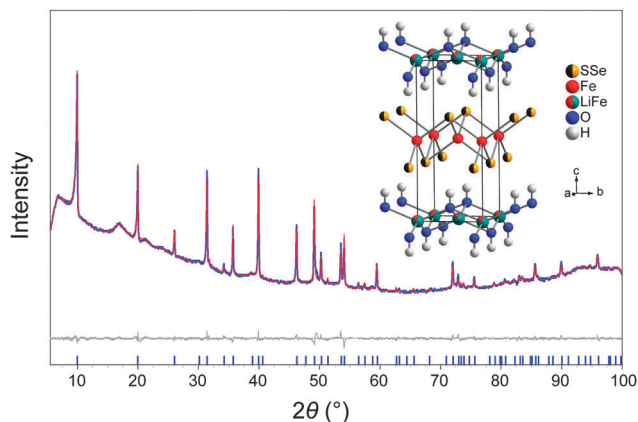


Fig. 1 X-ray powder pattern of $[(\text{Li}_{0.8}\text{Fe}_{0.2})\text{OH}]\text{FeS}$ (blue) with Rietveld-fit (red) and difference curve (gray). The feature at 18° is an artefact of the sample holder. Inset: crystal structure of $[(\text{Li}_{0.8}\text{Fe}_{0.2})\text{OH}]\text{Fe}(\text{S}_{1-x}\text{Se}_x)$.

issue of the crystal structure is the large U_{33} component of the thermal displacement ellipsoid at the Fe–Li mixed site. This was also observed by Sun *et al.*,⁹ and may be interpreted as split position with Li shifted along $[001]$ off the oxygen tetrahedra. Contrary to $[(\text{Li}_{1-x}\text{Fe}_x)\text{OH}](\text{Fe}_{1-y}\text{Li}_y)\text{Se}$ where the presence of Li or alternatively iron vacancies in the FeSe layer is discussed,⁷ refinements of X-ray single crystal diffraction data gives no indication of a Fe–Li mixed site or iron vacancies in sulphur doped compounds. Sun *et al.* suggested that the lattice parameter a decreases with decreasing amount of Fe vacancies in the FeSe layer.⁹ The lattice parameter a of $[(\text{Li}_{0.8}\text{Fe}_{0.2})\text{OH}]\text{FeS}$ is 370 pm, distinctly smaller compared to the selenides with $a = 378\text{--}382$ pm,⁹ thus a Fe–Li mixed site or iron vacancies in the FeS layer are rather unlikely. The lattice parameters and unit cell volumes of $[(\text{Li}_{0.8}\text{Fe}_{0.2})\text{OH}]\text{Fe}(\text{S}_{1-x}\text{Se}_x)$ increase linearly with the doping level x as shown in Fig. 2.

The linear trend of a and c over the whole doping range $0 \leq x < 1$ indicates homogeneous doping of sulphur, however, the pure sulphide slightly deviates from linearity. The shrinking of the unit cell due to the smaller ionic radius of sulphur is also known from *anti*-PbO type $\text{Fe}(\text{Se}_{1-z}\text{S}_z)$ ($z = 0\text{--}0.5$) with a possible solubility limit of $z \approx 0.3$.¹⁴ The critical temperature of

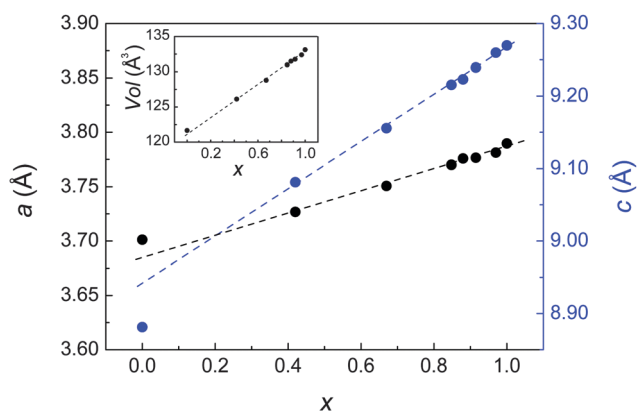


Fig. 2 Lattice parameters a (black) and c (blue) of $[(\text{Li}_{0.8}\text{Fe}_{0.2})\text{OH}]\text{Fe}(\text{S}_{1-x}\text{Se}_x)$. Inset: unit cell volume. Dashed lines are guides to the eye.

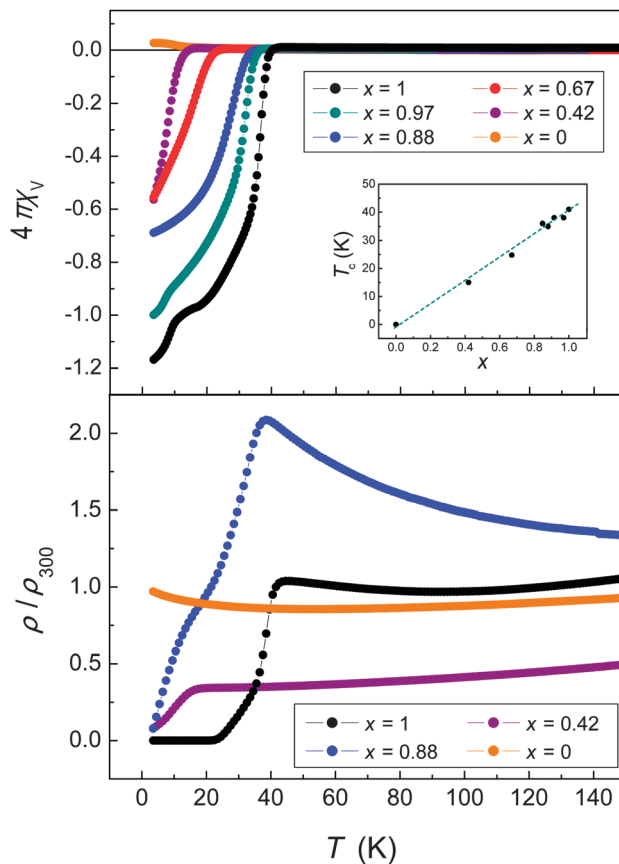


Fig. 3 Top: ac-susceptibility of $[(\text{Li}_{0.8}\text{Fe}_{0.2})\text{OH}]\text{Fe}(\text{S}_{1-x}\text{Se}_x)$. Inset: development of T_c with x . Bottom: dc resistivity for $x = 0$ (orange), 0.42 (magenta), 0.88 (blue) and 1 (black).

$\text{Fe}(\text{Se}_{1-z}\text{S}_z)$ increases up to 15.5 K for $x \leq 0.2$ due to chemical pressure.¹³ T_c decreases again at $x \geq 0.3$, thus it remains much smaller under chemical than under physical pressure (36 K).¹⁵ In contrast, sulfur-doping of $[(\text{Li}_{0.8}\text{Fe}_{0.2})\text{OH}]\text{Fe}(\text{S}_{1-x}\text{Se}_x)$ continuously decreases T_c linearly, until superconductivity is completely suppressed in the pure sulphide, as seen from the dc electrical transport measurements in Fig. 3.

The dc-resistivity of the pure selenide compound is weakly temperature dependent until it drops abruptly at 43 K (lower panel in Fig. 3). For $x = 0.88$ the resistivity drop is shifted to 37 K, and a shoulder appears at about 20 K, which is most probably due to the magnetic ordering of the Fe moments in the $(\text{Li}_{0.8}\text{Fe}_{0.2})\text{OH}$ layer (see below). The relatively large increase of resistivity above the superconducting transition is due to grain boundary effects, because cold pressed pellets have to be used owing to the temperature sensibility of the compounds. For $x = 0.42$ a distinct drop in resistivity is discernible at about 15 K, which is in good agreement with magnetic susceptibility measurements. As in this case the superconducting transition temperature coincides with the temperature range where the ferromagnetic ordering arises, the decrease in resistivity is rather broad. A tiny residual resistivity is observed, caused by grain boundary effects of the cold pressed pellets. Undoped $[(\text{Li}_{0.8}\text{Fe}_{0.2})\text{OH}]\text{FeS}$ shows no sign of a superconducting transition, which is in line



with the magnetic susceptibility measurements. However, a slight increase in resistivity can be observed at low temperatures, which might be again due to the emerging magnetic ordering in the $(\text{Li}_{0.8}\text{Fe}_{0.2})\text{OH}$ layer.

The enormous increase of T_c in $[(\text{Li}_{0.8}\text{Fe}_{0.2})\text{OH}](\text{Fe}_{1-y}\text{Li}_y)\text{Se}$ (43 K) in comparison to $\beta\text{-FeSe}$ (8 K) can be explained by electron doping from the hydroxide to the selenide layer.⁷ By substituting Se by S this electron doping does not change as Se and S ions have the same valence and the composition of the hydroxide layer remains constant. Though, the smaller S atoms lead to a chemical pressure effect, which influences superconductivity. Contrary to $\text{Fe}(\text{Se}_{1-z}\text{S}_z)$ where chemical pressure enhances superconductivity, we observe a decrease of T_c with increasing chemical pressure. Apparently in our case the geometry of the tetrahedral $\text{Fe}(\text{S}_{1-x}\text{Se}_x)$ layer is not further optimized. With increasing amount of S the unit cell volume and the Fe–Fe as well as the Fe–(Se,S) distances shrink. Contemplating the Ch–Fe–Ch bond angles of the FeCh_4 tetrahedra, a flattening of the $\text{Fe}(\text{S}_{1-x}\text{Se}_x)$ layers with increasing sulfur doping is observed (for the respective diagrams see ESI†). A definitive clue which parameter is crucial with respect to T_c cannot be given at this point. However, an enlargement of the unit cell with the respective opposite evolutions in geometry of the FeSe layer by substituting Se by Te appears promising.

The possible coexistence of superconductivity and ferromagnetism in the series $[(\text{Li}_{0.8}\text{Fe}_{0.2})\text{OH}]\text{Fe}(\text{S}_{1-x}\text{Se}_x)$ is of particular interest. In $[(\text{Li}_{0.8}\text{Fe}_{0.2})\text{OH}](\text{Fe}_{1-y}\text{Li}_y)\text{Se}$ magnetic ordering emerges from the iron ions in the hydroxide layer at about 10 K, well below the superconducting transition temperature at 43 K.⁷ While superconductivity becomes increasingly suppressed by sulphur doping, ferromagnetism persists over the whole substitution range. Fig. 4 shows the magnetic susceptibility of $[(\text{Li}_{0.8}\text{Fe}_{0.2})\text{OH}]\text{FeS}$ (black) and doped samples.

Selenium rich compounds show a strong diamagnetic signal in a 3 mT field analogous to $[(\text{Li}_{0.8}\text{Fe}_{0.2})\text{OH}](\text{Fe}_{1-y}\text{Li}_y)\text{Se}^7$ in the zero-field cooled mode (zfc, Fig. 4) where the shielding effect is strong. After field-cooling (fc, Fig. 4) the susceptibility becomes merely

slightly negative below T_c owing to the Meissner–Ochsenfeld effect before increasing to positive values at lower temperatures. This behaviour is known from $[(\text{Li}_{0.8}\text{Fe}_{0.2})\text{OH}](\text{Fe}_{1-y}\text{Li}_y)\text{Se}$ and a result of the coexistence of ferromagnetism and superconductivity.⁷ The susceptibility of undoped $[(\text{Li}_{0.8}\text{Fe}_{0.2})\text{OH}]\text{FeS}$ is throughout positive as superconductivity is completely suppressed. Nevertheless, for low temperatures we also observe a different signal in zfc and fc mode, respectively (see inset in Fig. 4). This splitting is typical for ferromagnetic ordering and caused by different domain formations in fc and zfc modes. Below $T_{\text{fm}} \approx 10$ K, the magnetic moments order spontaneously leading to an increase in magnetic susceptibility. In zfc mode, the domains are randomly distributed. Switching on the external field the domains tend to orientate along the field which is only partially accomplished. As a result the signal is lower compared to fc mode where the domains can align in the field during the cooling cycle.

The inverse susceptibility of $[(\text{Li}_{0.8}\text{Fe}_{0.2})\text{OH}]\text{FeS}$ at 2 T obeys the Curie–Weiss law with an effective magnetic moment of $4.98(1) \mu_B$ (see ESI†). This value is in good agreement with the theoretically expected $4.9 \mu_B$ for Fe^{2+} contrary to $5.9 \mu_B$ expected for Fe^{3+} .¹⁶ Thus, the situation of the iron ions in the hydroxide layer is unchanged. The electron transfer to the $\text{Fe}(\text{S}_{1-x}\text{Se}_x)$ layer and magnetic ordering in the $(\text{Li}_{0.8}\text{Fe}_{0.2})\text{OH}$ layer persist in $[(\text{Li}_{0.8}\text{Fe}_{0.2})\text{OH}]\text{Fe}(\text{S}_{1-x}\text{Se}_x)$ in the whole substitution range. The interplay of magnetism and superconductivity is further confirmed by magnetization measurements (Fig. 5).

The ferromagnetic hysteresis of $[(\text{Li}_{0.8}\text{Fe}_{0.2})\text{OH}]\text{Fe}(\text{S}_{1-x}\text{Se}_x)$ with $x > 0$ is superimposed by the magnetization known for hard type-II superconductors.⁷ The initial curves prove superconductivity in the Se containing compounds, which is in line with susceptibility measurements. Decreasing the amount of Se, the superconducting hysteresis continuously diminishes. As expected from susceptibility measurements, $[(\text{Li}_{0.8}\text{Fe}_{0.2})\text{OH}]\text{FeS}$ shows only the ferromagnetic ordering with a very narrow hysteresis typical for a soft ferromagnet. We suppose that the

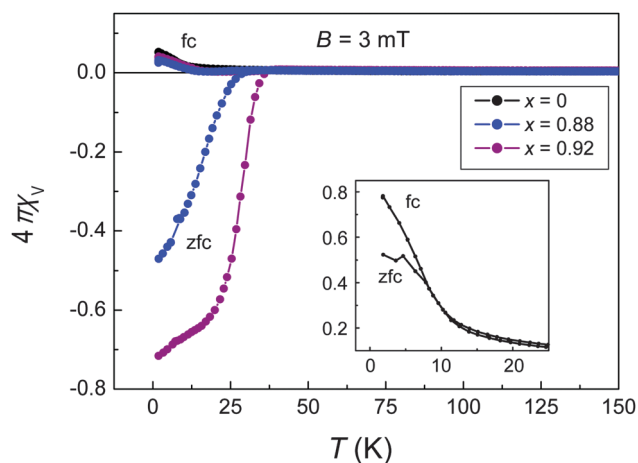


Fig. 4 Magnetic dc-susceptibility of $[(\text{Li}_{0.8}\text{Fe}_{0.2})\text{OH}]\text{Fe}(\text{S}_{1-x}\text{Se}_x)$ for $x = 0$ (black), 0.88 (blue) and 0.92 (magenta). Inset: magnification of the low-temperature part for $x = 0$.

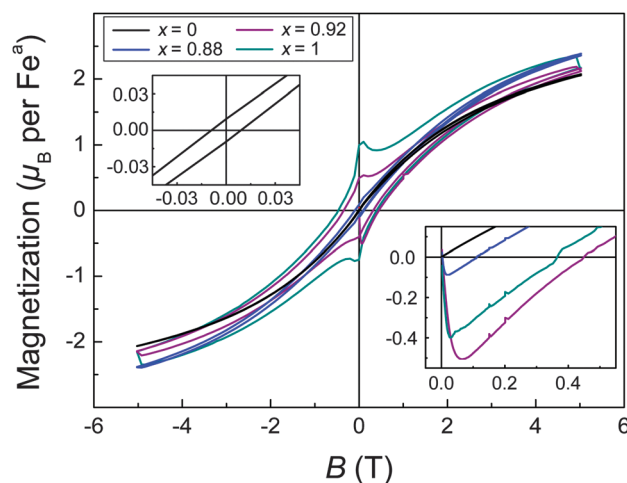


Fig. 5 Isothermal magnetization at 1.8 K of $[(\text{Li}_{0.8}\text{Fe}_{0.2})\text{OH}]\text{Fe}^b(\text{S}_{1-x}\text{Se}_x)$ for $x = 0$ (black), 0.88 (blue), 0.92 (magenta) and 1 (dark cyan). Inset: magnification of the low-field part showing the hysteresis for $x = 0$ (left inset) and the initial curves (right inset).



reason for this is the dilution of the magnetic iron ions in the hydroxide layer leading to small coupling.

$[(\text{Li}_{0.8}\text{Fe}_{0.2})\text{OH}]\text{FeS}$ and the series $[(\text{Li}_{0.8}\text{Fe}_{0.2})\text{OH}]\text{Fe}(\text{S}_{1-x}\text{Se}_x)$ were synthesized by hydrothermal methods and characterized by X-ray single crystal and powder diffraction, EDX and chemical analysis. Selenium-rich compounds show coexistence of magnetic ordering with superconductivity as known from the pure selenium compound. Sulphur doping decreases the critical temperature through chemical pressure until superconductivity is completely absent in $[(\text{Li}_{0.8}\text{Fe}_{0.2})\text{OH}]\text{FeS}$, while the ferromagnetic signature persists in the $[(\text{Li}_{0.8}\text{Fe}_{0.2})\text{OH}]$ layers. The Li:Fe ratio in the hydroxide layer and thus the charge transfer of 0.2 electrons from the hydroxide to the iron chalcogenide layers remains unchanged in $[(\text{Li}_{0.8}\text{Fe}_{0.2})\text{OH}]\text{Fe}(\text{S}_{1-x}\text{Se}_x)$ suggesting the chemical pressure effect of the smaller sulphide ions impedes superconductivity in $[(\text{Li}_{0.8}\text{Fe}_{0.2})\text{OH}]\text{FeS}$.

We thank for financial support by the German Research Foundation (DFG) within the priority program SPP1458 and by the FP7 European project SUPER-IRON (Grant no. 283204).

Notes and references

‡ Materials: Fe powder (Chempur, 99.9%), selenourea (Alfa Aesar, 99%), thiourea (Grüssing, 99%), LiOH (Fisher Scientific). X-ray powder diffraction was carried out using a Huber G670 diffractometer with Cu-K α_1 radiation ($\lambda = 154.05$ pm) and Ge-111 monochromator. Structural parameters were obtained by Rietveld refinement using the software package TOPAS.¹⁷ Single-crystal analysis was performed on a Bruker D8-Quest diffractometer (Mo-K α_1 , $\lambda = 71.069$ pm, graphite monochromator). The structure was solved and refined with the Jana2006 program package.¹⁸ Chemical compositions were additionally determined by energy-dispersive X-ray analysis (EDX) as well as by chemical methods using ICP-AAS and combustion analysis. Magnetic properties were examined with a Quantum Design MPMS-XL5 SQUID magnetometer, whereas superconductivity was examined in ac-susceptibility measurements.

Temperature-dependent resistivity measurements were carried out on cold pressed pellets using a standard four-probe method.

- 1 M. Sgrist and K. Ueda, *Rev. Mod. Phys.*, 1991, **63**, 239–311.
- 2 R. Hackl, *Z. Kristallogr.*, 2011, **226**, 323–342.
- 3 D. Johrendt and R. Pöttgen, *Angew. Chem., Int. Ed.*, 2008, **47**, 4782.
- 4 D. Johrendt, *J. Mater. Chem.*, 2011, **21**, 13726–13736.
- 5 G. R. Stewart, *Rev. Mod. Phys.*, 2011, **83**, 1589–1652.
- 6 L. J.-X. Yu Shun-Li, *Chin. Phys. B*, 2013, **22**, 087411.
- 7 U. Pachmayr, F. Nitsche, H. Luetkens, S. Kamusella, F. Brückner, R. Sarkar, H.-H. Klauss and D. Johrendt, *Angew. Chem., Int. Ed.*, 2015, **54**, 293–297.
- 8 X. F. Lu, N. Z. Wang, H. Wu, Y. P. Wu, D. Zhao, X. Z. Zeng, X. G. Luo, T. Wu, W. Bao, G. H. Zhang, F. Q. Huang, Q. Z. Huang and X. H. Chen, *Nat. Mater.*, 2014, DOI: 10.1038/nmat4155.
- 9 H. Sun, D. N. Woodruff, S. J. Cassidy, G. M. Allcroft, S. J. Sedlmaier, A. L. Thompson, P. A. Bingham, S. D. Forder, S. Cartenet, N. Mary, S. Ramos, F. R. Foronda, B. H. Williams, X. Li, S. J. Blundell, and S. J. Clarke, *Inorg. Chem.*, 2015, DOI: 10.1021/ic5028702.
- 10 F. C. Hsu, J. Y. Luo, K. W. Yeh, T. K. Chen, T. W. Huang, P. M. Wu, Y. C. Lee, Y. L. Huang, Y. Y. Chu, D. C. Yan and M. K. Wu, *Proc. Natl. Acad. Sci. U. S. A.*, 2008, **105**, 14262–14264.
- 11 M. Burrard-Lucas, D. G. Free, S. J. Sedlmaier, J. D. Wright, S. J. Cassidy, Y. Hara, A. J. Corkett, T. Lancaster, P. J. Baker, S. J. Blundell and S. J. Clarke, *Nat. Mater.*, 2013, **12**, 15–19.
- 12 A. Krzton-Maziopa, E. V. Pomjakushina, V. Y. Pomjakushin, F. v. Rohr, A. Schilling and K. Conder, *J. Phys.: Condens. Matter*, 2012, **24**, 382202.
- 13 X. F. Lu, N. Z. Wang, X. G. Luo, G. H. Zhang, X. L. Gong, F. Q. Huang and X. H. Chen, *Phys. Rev. B: Condens. Matter Mater. Phys.*, 2014, **90**, 214520.
- 14 Y. Mizuguchi, F. Tomioka, S. Tsuda, T. Yamaguchi and Y. Takano, *J. Phys. Soc. Jpn.*, 2009, **78**, 074712.
- 15 S. Medvedev, T. M. McQueen, I. A. Troyan, T. Palasyuk, M. I. Erements, R. J. Cava, S. Naghavi, F. Casper, V. Ksenofontov, G. Wortmann and C. Felser, *Nat. Mater.*, 2009, **8**, 630–633.
- 16 H. Lueken, *Magnetochemie: Eine Einführung in Theorie und Anwendung*, Teubner, Stuttgart, 1999.
- 17 A. Coelho, *COELHO Software*, Brisbane, 2007.
- 18 V. Petricek, M. Dusek and L. Palatinus, *Structure Determination Software Programs*, Institute of Physics, Praha, Czech Republic, 2009.

